national accelerator laboratory

TM-334A
2791.000

THE HEIM COLUMN

A Low Heat Leak Temperature Stabilized Support

J. R. Heim

December 10, 1971

ABSTRACT

The design and analysis of a low heat leak temperature stabilized column type support is presented. Engineering design formulas have been developed for a three tube composite column which uses the cryostat liquid nitrogen radiation shield as a heat sink. Also, the design concept and method of analysis for the general case using many tubes with or without heat sinks is also developed. These simple structural elements conduct negligible amounts of heat to the supported cold mass and may be designed to shrink, grow or remain unchanged in height when cooled to operating conditions. The three tube specimen presented herein has a collapse load of 9,000 Kg and a heat leak of less than eleven milliwatts.

Operated by Universities Research Association Inc. Under Contract with the United States Atomic Energy Commission

INTRODUCTION

Most superconducting magnet coils operate in a liquid helium environment at temperatures near 4°K. Since the operating efficiency of these devices is directly related to the heat transferred into the helium pool, much cryostat design effort is devoted to minimizing heat leaks. One of the major heat leak paths for a large superconducting magnet is the primary structure which supports the cold mass. The composite column described herein has been designed to be used as such with good load carrying capability and low heat leak. The test specimen shown in Fig. 1 has been

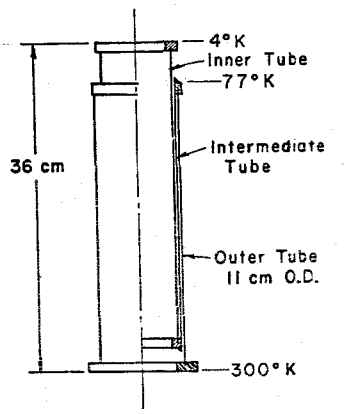

Fig. 1 Test Specimen

sized to carry a 1,000 Kg axial load at 4°K with a heat leak of less than 11 milliwatts and no shrinkage when cooled down. The top end of the column is attached to a liquid helium chamber and the bottom end is attached to the vacuum jacket wall at room temperature. The joint between the intermediate and outer tubes is thermally sinked to a liquid nitrogen radiation shield at 77°K.

THREE TUBE COLUMN

This example is the basic form of a composite column in that a minimum number of tubes have been used and the intermediate tube is forced to a sink temperature.

Design Concept

The column shown is made with 3 tubes and the following considerations:

Geometry Consideration. A decrease of the intermediate tube length will increase the overall column height.

Materials Consideration. The individual tubes may be made from different materials with correspondingly different thermal expansion coefficients.

If one selects materials such that the thermal contraction of the intermediate tube is equal to the sum of the contractions of the inner and outer tubes, the overall column height will not change when the column is cooled down to operating conditions. Thus, all alignments may be done when the magnet is installed and the alignments will not be lost when the magnet is cooled down.

For superconducting magnet coil support applications an excellent combination of inexpensive materials may be chosen which satisfies the above temperature considerations and also has low heat conduction. The inner and outer tubes are made of epoxy glass laminates and the intermediate tube is made of aluminum. Both materials are readily available in a wide variety of tube sizes.

Construction Details

The test specimen shown was constructed using 6061 T6 aluminum for the intermediate tube and NEMA grade G-10[1] epoxy fiberglass for the inner and outer tubes. Both G-10 tubes have a .16 cm wall thickness since this was the thinnest tube wall thickness manufactured using normal shop practice. A .32 cm wall thickness was chosen for the aluminum tube to assure good tube-to-flange welds. Four aluminum flanges were machined with .6 cm deep grooves to accept the G-10 tubes and two of these flanges were welded to both ends of the aluminum tube as shown in Fig. 2. Prior to bonding

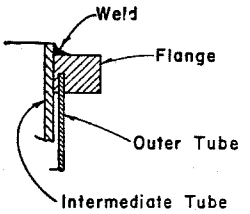

Fig. 2 Typical Joint

with epoxy all aluminum bonding surfaces were chemically etched with a sodium dichromate sulfuric acid solution while the G-10 bonding surfaces were lightly sanded and wiped with a cleaning agent. All aluminum to G-10 joints were bonded together with a low temperature epoxy[2]. Also, temporary spacers were used between tubes to maintain concentricity while the epoxy cured. After curing, the top and bottom flange surfaces were final machined perpendicular to the column center line.

Thermal Analysis

Computation of the heat transferred up the inner tube and into the helium chamber is fairly straight forward. Several layers of superinsulation were wrapped on all surfaces to limit radiant heat transfer. Therefore, radiant heat transfer was neglected to simplify analysis. The thermal conductivity of aluminum is much greater than that of epoxy glass laminates, therefore, the aluminum tube was assumed to be an isothermal surface. Since the thermal conductivity of epoxy glass laminates is fairly constant at low temperatures, Fouriers conduction equation may be integrated directly to yield the familiar form

$$\dot{Q} = -kA \frac{T_T - T_B}{\ell_3}$$

where $\dot{Q}$ = heat flow into helium chamber

k = thermal conductivity of inner tube

A = cross sectional area of inner tube

ℓ_3 = length of inner tube between flanges

T_T = temperature at top end (approx. 4°K)

T_B = temperature at bottom end (approx. 80°K)

Since low temperature properties were not available for the G-10 material used for the inner and outer tubes, the thermal conductivities and coefficients of expansion of two known epoxy glass laminates[3] were averaged and used for preliminary analysis. Using these average properties a temperature profile was developed which satisfied boundary conditions and the incremental contractions were summed to obtain an

estimate of the total height change. The results of these calculations showed a column growth of .04 cm and a heat leak to the helium vessel of 11 milliwatts.

Structural Analysis

Collapse Load. The inner and outer G-10 tubes are loaded in compression and should be checked for buckling. The buckling stress for a thin walled circular tube axially loaded may be calculated using the approximation[4]

$$S' = .3\ Et/r$$

where S' = buckling stress

E = modulus of elasticity

t = wall thickness

r = mean radius

If the buckling stress is lower than the compressive yield strength for the material being considered, the buckling stress value should be used to calculate the column collapse load.

$$P_c = A\ \sigma$$

where P_c = collapse load (axial)

A = cross sectional area of tube

σ = failure stress (compressive yield strength on buckling stress, whichever is smaller)

Column Stiffness

By definition a column is a vertical support member normally loaded in compression. However, other loading conditions must be considered:

1. Handling and transport

2. Unbalanced magnetic forces applied to the superconducting coil

3. Shock and vibration environments

For all of the above conditions column stiffness is an important structural property which must be considered if support system capability is to be reasonably evaluated.

Axial Stiffness. The axial column deflection δ, due to the application of axial compressive force P may be calculated using[5]

$$\delta = P \sum_{n=1}^{3} \frac{\ell_n}{A_n E_n}$$

where δ = axial deflection

P = applied load (unit load used for calculating stiffness)

ℓ = tube length between flanges

A = tube cross sectional area

E = modulus of elasticity of material

n = subscript identifying outer, intermediate and inner tubes respectively

Lateral Stiffness (bottom end fixed, top end free). The lateral influence coefficient for this condition may be determined by using the unit load method[6].

$$\delta = \int \frac{m^2 d\ell}{EI} + \int \frac{kv^2 d\ell}{AG}$$

where δ = top lateral deflection for unit lateral force applied at same location

E = modulus of elasticity of material

I = area moment of inertia of Section ($\pi r^3 t$ for a thin circular section)

$d\ell$ = incremental unit of length (longitudinal)

k = shape factor (2 for a thin walled circular section)

m = moment distribution due to unit lateral load

v = shear distribution due to unit lateral load

G = modulus of rigidity

integrating the above for the 3 tube case yields

$$\delta = \frac{\ell_1}{3E_1I_1}\left[(\ell_1 + \ell_3 - \ell_2)^2 + (\ell_3 - \ell_2)^2 + (\ell_1 + \ell_3 - \ell_2)(\ell_3 - \ell_2)\right] + \frac{k\ell_1}{A_1G_1} + \frac{\ell_2}{3E_2I_2}\left[\ell_3^2 + (\ell_2 - \ell_3)^2 - \ell_3(\ell_2 - \ell_3)\right] + \frac{k\ell_2}{A_2G_2} + \frac{\ell_3^3}{3E_3I_3} + \frac{k\ell_3}{A_3G_3}$$

Lateral Stiffness (bottom end fixed, top end free to translate but no rotation). The application of column top end rotational constraints will be explained later when column systems are described. The column lateral stiffness change due to this top end rotational constraint is readily determined using the following method. A unit lateral load is applied to the column free end as before and the angular deflection of the free end due to this unit lateral load may be calculated using elementary beam theory. Then an end moment is applied to restore parallelism between the top and bottom flanges. The lateral deflection due to

this end moment is then subtracted from the "top end free" case previously solved to obtain the complete solution. The lateral stiffness of a composite column with the above rotational constraint is approximately three times greater than the free ended column.

Tests and Results

Cold Test

To verify the basic concept a simple test was set-up as shown in Fig. 3.

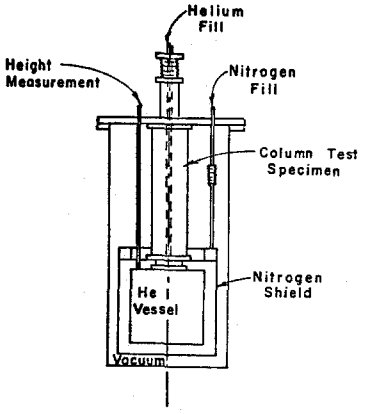

Fig. 3 Column Cold Test

The insulating vacuum chamber was pumped down and maintained below 10^{-1} millitorr for all testing. A column free height measurement was taken prior to filling with liquid nitrogen and helium. After filling with cryogens column height, temperature, and helium boil-off measurements were taken periodically for several days. Height measurements were taken with a brass rod which was inserted into the cryostat and measured while still at room temperature. Helium boil-off measurements were taken with a helium flow meter. Temperatures were measured with copper

constantan thermocouples using a liquid nitrogen cooled reference junction.

The final results showed a maximum temperature differential along the intermediate tube of 1.5°K with a total cryostat helium boil-off of .11 liquid liters per hour. Since the calculated column heat leak represented about one tenth of the total boil-off measured which seemed reasonable, no attempt was made to isolate the column boil-off from the total.

Although the column height changed appreciably during and immediately after cooldown, the final height after steady state was reached was identical to the room temperature height. This disagreement between measured and calculated height change was probably due to differences in the epoxy glass laminate properties data used for preliminary analysis and the true properties of G-10. After warm-up, the column height was again measured and no change was observed.

Room Temperature Tests

After completion of the cold test, the same specimen was removed from the cryostat and set-up for room temperature lateral stiffness tests as shown in Figs. 4 and 5.

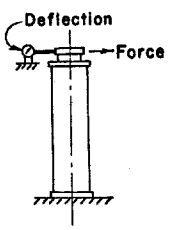

Fig. 4 Lateral Stiffness Test, Top End Free

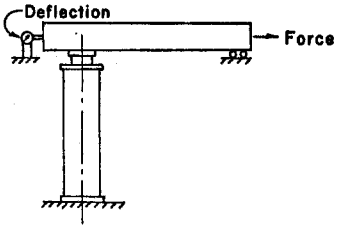

Fig. 5 Lateral Stiffness Test, Top End Free to Translate, but no rotation

The results of these tests are shown in Fig. 6.

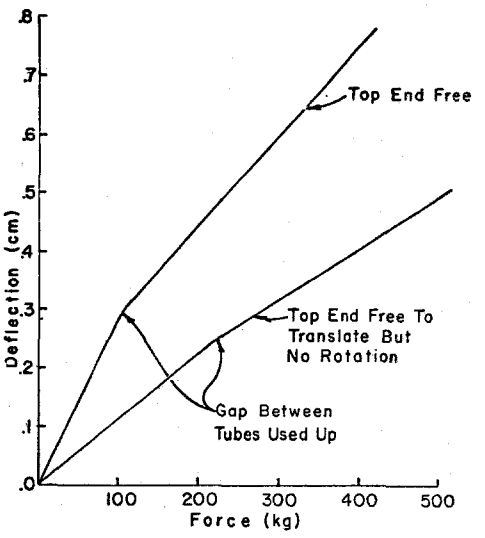

Fig. 6 Column Lateral Stiffness Test Results

Upon completion of the lateral stiffness tests the same test specimen was tested to failure by application of axial load. The results of this test are shown in Fig. 7.

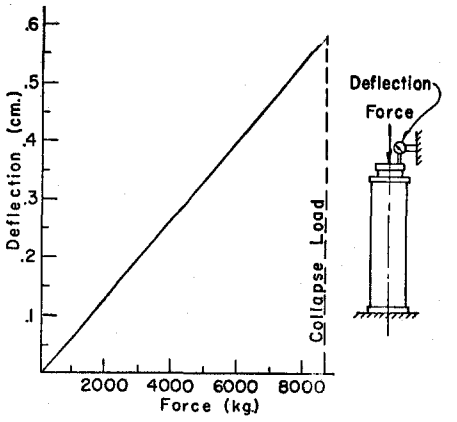

Fig. 7 Axial Stiffness and Collapse Load Test Results

THE GENERAL CASE

For many cryogenic support applications the basic three tube column may not be suitable in that liquid

nitrogen radiation shielding may not be used and also the space available for support structure may be limited. For such applications the low heat leak and temperature stabilization features of the previously described column may still be achieved by using many tubes of shorter length. The composite column shown in Fig. 8 using nine

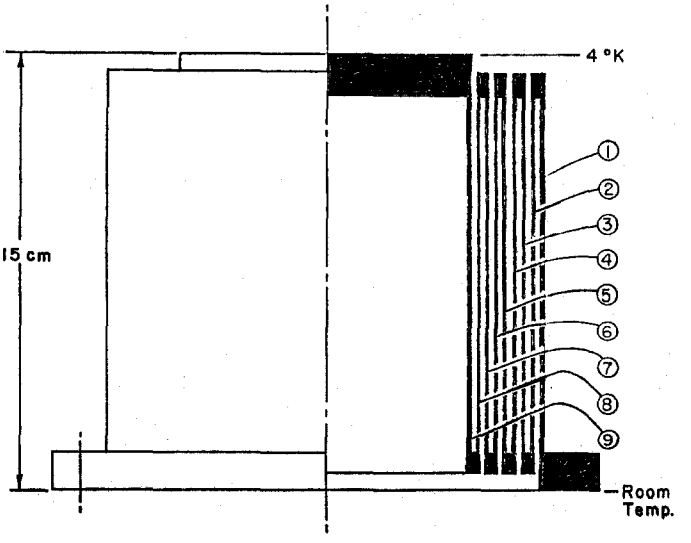

Fig. 8 Nine Tube Composite Column

concentric tubes has been chosen as a typical example for analysis. Although a wide variety of materials may be used for such column construction the following discussion is limited to two representative materials only. All metallic parts are made of 6061 aluminum in the T6 condition and all nonmetallic parts are made from epoxy glass laminates. Two types of epoxy glass laminates have been considered for which low temperature data is available. Also, to simplify analysis all tubes were assumed to have the same cross sectional area of 5 square

centimeters and radiant heat transfer between tubes has been neglected. The structural analysis approach used for the three tube case may also be used for the many tube general case. Therefore, the following discussion considers thermal analysis only.

The following approach was used for thermal analysis. An epoxy glass laminate rod of uniform cross sectional area and unknown length is sinked to room temperature at one end and 4°K at the other end. A conduction heat flow rate per unit cross sectional area is assumed to flow into the rod at the room temperature end and using thermal conductivity vs. temperature data from reference 3 the incremental rod length corresponding to unit incremental temperature decrease was calculated using Fouriers conduction equation. These data were then normalized to dimensionless length and are shown for two epoxy glass laminates in Fig. 9.

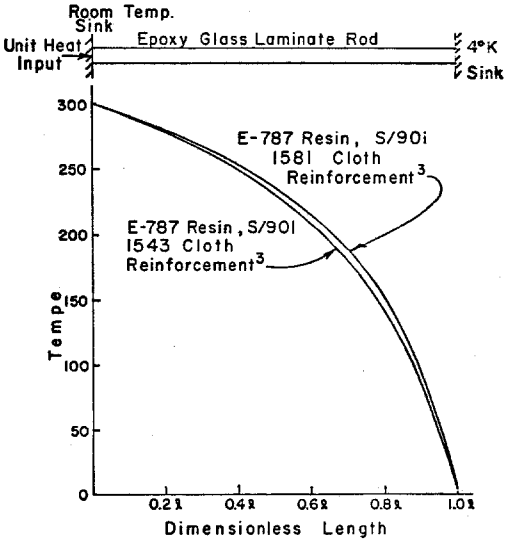

Fig. 9 Characteristic Temperature Profiles

Note that these temperature profiles are independent of cross sectional area and length (assuming uniform cross sectional area and conduction heat transfer only) whose shape is characterized by the thermal conductivity variation with temperature only. Therefore, segments of the curve may be used to represent the temperature profile between any two sinks chosen arbitrarily. Thus, if one cuts the temperature curve at 77°K, the profile to the left is representative of the temperature variation between a liquid nitrogen sink and room temperature and similarly the profile to the right is representative of the temperature variation between a liquid nitrogen sink and 4°K.

Also consider, the above rod may be cut at any location along the ℓ-axis and a length of aluminum may be added without change to the epoxy glass laminate temperature profile. Since the thermal conductivity of aluminum is much greater than that of epoxy glass laminates the position of the temperature curve to the right of the cut will be shifted horizontally but both parts of the epoxy glass laminate temperature profile will remain unchanged in shape.

To complete the thermal analysis, length changes corresponding to the characteristic temperature profiles were calculated and the heat transferred across the 4°K boundary was determined by measuring the slope of the temperature curve at this boundary.

Table I presents the results of these calculations which shows the column heat leak and height change for seven different conditions.

Table I. Nine Tube Composite Column Analytical Results

Tube Materials	LN_2 Intercept Location Tube Number Fig. 8	Epoxy Glass Laminate Material[3] E-787 Resin S/901 1543 Cloth Reinforcement		E-787 Resin S/901 1581 Cloth Reinforcement	
		Heat Leak (Milliwatts)	Column Growth (cm)	Heat Leak (Milliwatts)	Column Growth (cm)
Even numbered tubes made of aluminum, odd numbered tubes made of epoxy glass laminates	none	60	.05	69.4	.02
	8	27.6	.06	27.8	.03
	6	13.8	.09	13.9	.05
	4	9.2	.11	9.3	.06
	2	6.9	.14	6.9	.08
All tubes epoxy glass laminates	none	34.9	-.008	38.5	-.015
Tube Number 2 aluminum all others epoxy glass laminates	2	3.9	.028	4.0	.011

Note: Negative column growth indicates shrinkage.

COLUMN SUPPORT SYSTEMS

For most cryogenic support applications a single column is not adequate and a system of columns would be used. Several column support systems concepts have been designed for large superconducting magnets to be used at National Accelerator Laboratory. The following discussion describes systems of two or more columns being used.

For all multiple column systems flexural hinges have been used on one or more columns to compensate for thermal contraction of the helium vessel. These flexural hinges are made of 6AL4V titanium which has a high yield strength to modulus of elasticity ratio corresponding to a high elastic strain capability. (See Appendix)

Two Column System

A simple two column system which is presently being used on a 3 meter quadrupole magnet is shown in Fig. 10.

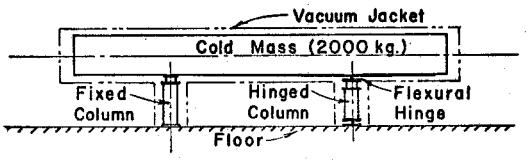

Fig. 10 Two-Column System for Three-Meter Quadrupole Magnet

The column on the left which is designated the "fixed column" has the top end bolted to the helium chamber and the bottom end bolted to the vacuum jacket base. The column on the right which is designated the "hinged column" is attached similarly but flexural hinges have been used both top and bottom to compensate for helium vessel shrinkage relative to the vacuum jacket. Note that the ends of the fixed column are constrained against rotation in the plane of the paper and this column would be treated analytically as "bottom end fixed, top end free to translate but no rotation" in the paper plane. However, normal to the plane of the paper both columns would be treated analytically as "bottom end fixed, top end free".

Therefore, the hinged column does not degrade support system lateral stiffness in the plane of the paper, in fact, the support system stiffness is greater in that plane.

Three Column Systems

Two support systems concepts using three columns have been developed. The six meter long dipole magnet shown in Fig. 11 could be used as a beam transport bending

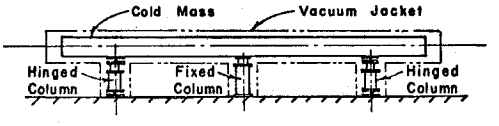

Fig. 11 Three-Column System for Six-Meter Dipole Magnet

magnet. This support system is well suited for a long slender cold mass. Note that this support system is well balanced in that the lateral stiffness in both directions are approximately equal.

Fig. 12 shows a large aperature dipole magnet which will be used as a particle spectrometer magnet. This magnet

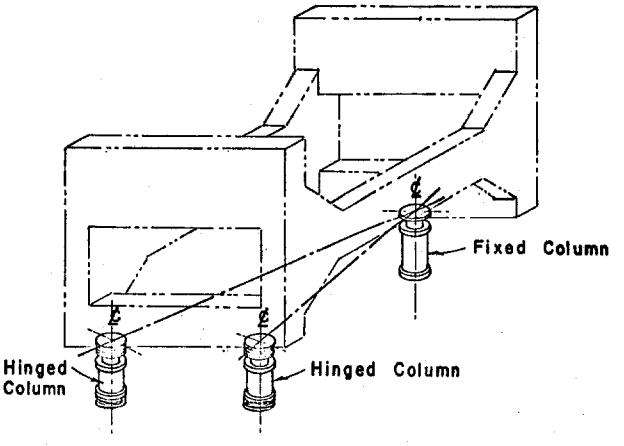

Fig. 12 Three-Column System for Spectrometer Magnet

is presently in the final construction stage and will be tested in the near future.

A fixed column has been used at the far end and two hinged columns have been used at the near side. Note that the flexural hinge axes of rotation have been aligned normal to a vertical plane which contains both a hinged column centerline and the fixed column centerline.

Four Column System

Fig. 13 shows a larger particle spectrometer magnet

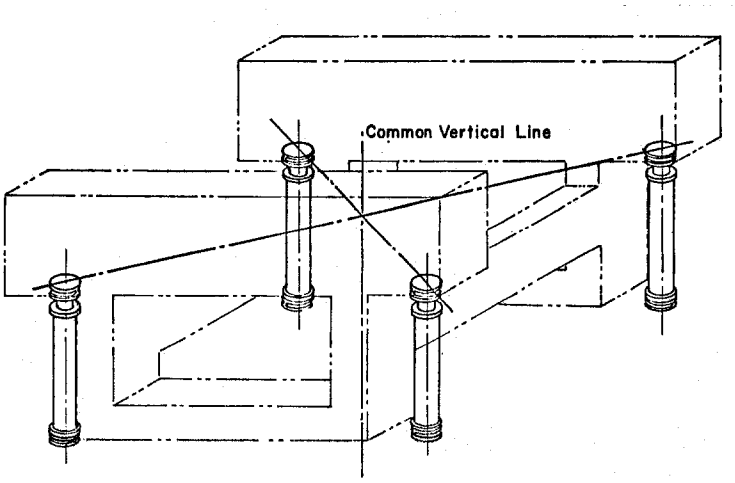

Fig. 13 Four-Column System for Spectrometer Magnet

which is now being designed. This support system concept uses many hinged columns and no fixed columns. Note that all flexural hinge axes of rotation have been aligned normal to vertical planes which intersect at a vertical line common to all such planes. For the four column system shown the system is balanced by locating this common vertical line equidistant from the four column centerlines.

SUMMARY AND FUTURE PLANS

Summarizing we may say that composite columns can be used to support large cold masses with controlled thermal distortion and small heat leak through the support structure. These devices are especially well suited for large superconducting magnet applications when the magnet is floor mounted. The support structure may then be an integral part of the vacuum jacket with a composite column conveniently housed inside.

For other applications where the volume available for support structure is limited, shorter composite columns made with many tubes may be used, however, joint design should be studied and tested in more detail (e.g. the three tube column epoxy joint tested was loaded in compression only while a many tube column design may require epoxy glass laminate tension joints).

Finally, a wide variety of low conductivity materials with good mechanical properties suitable for column construction are available but low temperature data on these materials is very limited or non-existent. Therefore, a series of simple materials tests has been planned to evaluate these materials.

ACKNOWLEDGMENTS

The author wishes to acknowledge E. H. Scholefield for his assistance in hardware design and preparation of this paper, H. L. Hart and J. J. Santori who helped with hardware fabrication and testing, and R. W. Fast for his helpful discussions and support through the course of this work.

APPENDIX

Flexural Hinge Design and Analysis

The hinge web geometry of the test specimen shown in Fig. 14 was sized conservatively to be used with the three tube column described previously. The specimen was made from 6AL4V titanium round stock in the annealed condition with no heat treatment after machining.

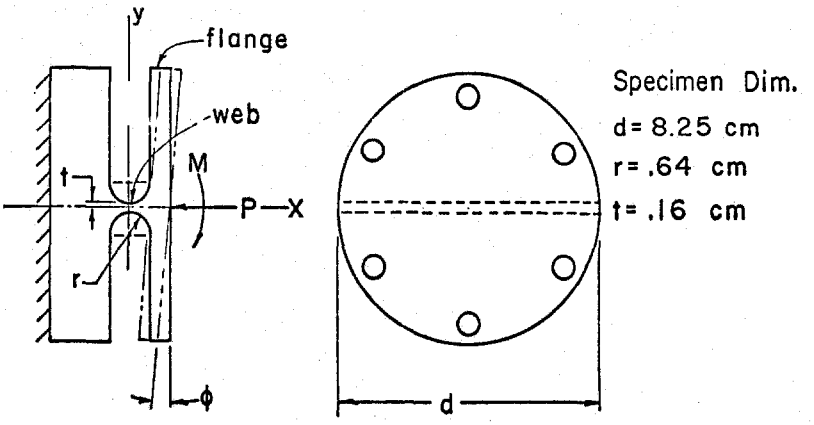

Fig. 14 Flexural Hinge Test Specimen

The following analytical approach assumes that the assumptions commonly made in the development of plate theory[7] hold to a reasonable degree of accuracy for the web shape shown. Following good engineering practice the maximum moment M which may be applied for elastic behavior of the hinge web is

$$M_{max} = \frac{2}{3} \sigma_y \, dt^2$$

where σ_y = yield strength of material

d = web length

t = one half minimum web thickness

The following expression was then developed for the hinge rotation corresponding to M_{max}

$$\phi_{M_{max}} = \frac{2\sigma_y (1 - \nu^2)}{E} \left(\frac{t}{r}\right)^2 f\left(\frac{t}{r}\right)$$

where ν = poissons ratio

E = modulus of elasticity

r = web radius

$$f\left(\frac{t}{r}\right) = \int_o^r \frac{d\left(\frac{x}{r}\right)}{\left\{1 + \frac{t}{r} - \left[1 - \left(\frac{x}{r}\right)^2\right]^{\frac{1}{2}}\right\}^3}$$

The above integral was then evaluated numerically and a plot of $f\left(\frac{t}{r}\right)$ as a function of $.05 < \frac{t}{r} < 1.0$ is presented in Fig. 15.

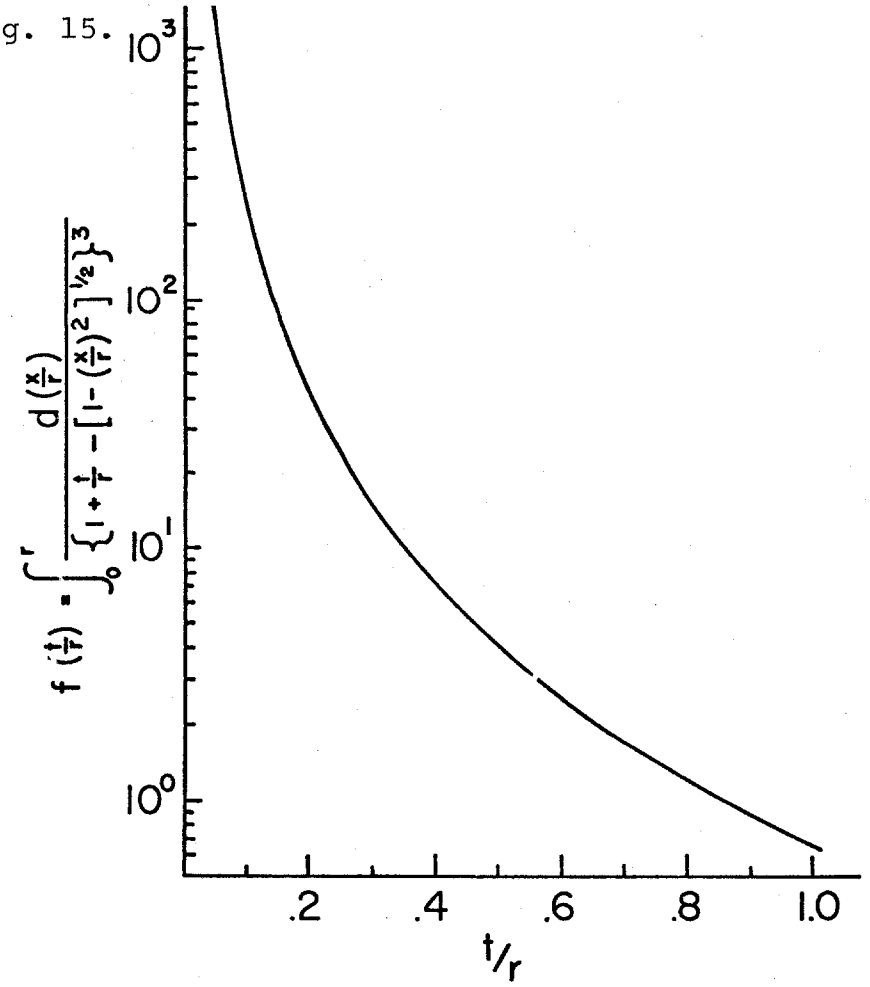

Fig. 15 $f\left(\frac{t}{r}\right)$ Integral Value

For most column support applications the flexural hinge must transmit an axial force P which reduces the hinge rotational limit for elastic behavior. The last term on the right hand side of the following equation accounts for this applied load.

$$\phi_{max} = \frac{2\sigma_y (1 - \nu^2)}{E} \left(\frac{t}{r}\right)^2 f\left(\frac{t}{r}\right)\left(1 - \frac{P}{2dt\sigma_y}\right)$$

Where ϕ_{max} is the maximum angular deflection that the hinge will resist elastically. If the hinge is rotated through an angle greater than ϕ_{max} the hinge web will exhibit plastic deformation.

Using this equation and the web dimensions shown in Fig. 14 the test specimen rotational limit ϕ_{max} was calculated to be .023 radians for P = 0. The specimen was then tested and the web yield deflection due to the application of moment was measured to be .025 radians. Although the measured deflection was approximately 8% greater than the calculated value this agreement is considered good. One would expect the measured rotation to be greater since the hinge flange and mounting hardware are not infinitely rigid. (i.e. the hinge web was assumed to be the only flexible element in the system.)

REFERENCES

[1]National Electrical Manufacturers Association Standard for Laminated Plastics. The G-10 tubing used was supplied by Richardson Company, 300 South Seventh Street, DeKalb, Illinois 60115.

[2]Narmco 3170 epoxy resin with 7133 curing agent supplied by Crest Products Company, 14939 Dillow Street, Westminster, California 92683.

[3]Schwartzberg, F. R., et al, Cryogenics Materials Data Handbook, AD609562, The Martin Company, Denver, Colorado, latest revision August 1968, pgs. H.1.t, H.1.V and A.13.t.

[4]Roark, R. J., Formulas for Stress and Strain, Fourth Edition, pg. 352, Case 25.

[5]Roark, R. J., Formulas for Stress and Strain, Fourth Edition, pg. 80, Equation 3.

[6]Roark, R. J., Formulas for Stress and Strain, Fourth Edition, pg. 98, Equation 6, and pg. 129, Equation 16.

[7]Timoshenko, S. and Woinowsky-Krieger, S., Theory of Plates and Shells, Second Edition, Pgs. 4, 5 and 6.

national accelerator laboratory

TM-334-B
2750.0

SUPERCONDUCTING COIL TRAINING AND INSTABILITIES DUE TO THE BAUSCHINGER EFFECT

J. R. Heim

June 13, 1974

ABSTRACT

For many years the marginal performance of many superconducting coils has been tolerated because of a lack of understanding as to the cause of the observed effects. Study efforts and laboratory experiments have identified electrical losses associated with coil performance but unidentified mechanical losses which generate heat and degrade coil performance have been overlooked. This manuscript describes the inelastic behavior of superconducting composite conductors which must be considered if coil performance is to be reasonably evaluated. The experimental techniques used and the results obtained are described. The significance of the results is assessed and methods of eliminating mechanical losses are described. A new process for stabilizing the superconductor matrix metal, the PWP process (post wind preload) is presented.

Operated by Universities Research Association Inc. Under Contract with the United States Atomic Energy Commission

INTRODUCTION

Most superconducting coils operate in a liquid helium environment at temperatures near 4°K. Since the current carrying capability of the superconductor is strongly dependent upon the superconductor temperature much effort has been devoted to maintaining the superconductor temperature as close as possible to the helium bath temperature. These methods include:

(1) helium flow channels built into the coil structure to allow the coolant to come into direct contact with the conductor

(2) high conductivity metallic fins (heat drains) sandwiched between layers of wire to conduct the generated heat into the helium bath

(3) loaded epoxies to conduct heat through the coil structure and into the helium bath

The first of these methods (flow channels) has been used extensively in the past with good results but inherent with this type of construction one is satisfied with lower current densities in the coil and the resultant coil volume is large. For many applications coil volume is not a constraint and the above construction is adequate. However, for many other applications small coil volume is of great importance and the latter 2 methods of construction are used. The last method of construction (potted coils) approaches the ideal coil in that the finished product is rugged and

capable of carrying high current densities, but the methods of analysis must be refined to accommodate a less conservative design.

Let us interpret the last sentence in straight forward engineering language. If we sacrifice cooling capability for higher current densities we must identify and understand all sources of heat or the stability calculations will not accurately predict coil performance. Temperature - specific heat and temperature - enthalpy curves show the heat content of conductor materials to be very small at liquid helium temperatures with the heat content approaching zero as temperature decreases. Therefore, small sources of heat may not be neglected. i.e. seemingly small sources of heat may produce a significant temperature rise and coil stability is dominated by conductor temperature. All heat sources must be accounted for if coil stability is to be guaranteed.

One of the major heat sources which has been overlooked is a mechanical loss due to inelastic behavior of the matrix metal used to stabilize the superconductor. The following discussion identifies these losses and describes their effect on coil stability.

ANALYTICAL APPROACH

The following work started out as a simple effort to explore the limits of a coil type construction which has been used successfully to build large superconducting magnets for high energy physics experiments. To refine the methods of analysis used to design these coils the first step was to

determine the prestressed condition of the coil conductor just prior to charging for the first time. Simplifying assumptions had been made in the past and the validity of these assumptions has been investigated with significant results.

A representative superconducting wire specimen was chosen for analysis and subsequent testing. Specimen wire data is shown below.

Material - niobium titanium (N_bT_i) with a copper matrix

wire diameter - .040 inches

copper to superconductor ratio - 4/1

filament diameter - .002 inches

number filaments - 84

twist pitch - 2 per inch

The character of the partners making up the composite was then considered. Copper is a good superconductor stabilizing metal in the softened condition but a poor structural material. Niobium titanium on the other hand is radically different. N_bT_i is a tough metal with a very high elastic strain capability. Also, the expansion coefficients of the two metals differ by more than a factor of two. In line with the above considerations, simplifying assumptions as to the residual stress condition of the composite components after the manufacturing process is not justified.

Manufacturing Process Effects

1 - drawing

Looking back into the wire manufacturing processes one can choose a stage where the stress condition of both components is known fairly well. The obvious choice is the final draw immediately following twisting. This final draw is performed to "set the twist". An initial assumption then followed:

AT FINAL DRAW BOTH METALS EXIT THE DRAWING DIE STRESSED TO THEIR ULTIMATE STRENGTHS AS SHOWN

N_bT_i	175,000 p.s.i.
Cu	45,000 p.s.i. (true stress)

2 - annealing

The next manufacturing process is a heat treatment to soften the copper. This anneal process is considered "company proprietary information" by most manufacturers but similarity of processes justifies assumptions. The following heat treatment assumptions were made:

(1) THE COPPER IS SOFTENED TO THE FULL ANNEAL CONDITION

(2) THE WIRE IS WOUND TIGHTLY ON A STEEL SPOOL FOR HEAT TREATMENT

Using the above assumptions we may now proceed to calculate the internal stress condition of the wire. First, we assume that the N_bT_i is uniformly distributed throughout the

copper. Second, we neglect the effects of twisting (twisting effects will be considered later). The internal stress is best described by the average strain differential ($\delta\varepsilon$) between the N_bT_i and copper as

$$(1)\quad \delta\varepsilon = \varepsilon_s - \varepsilon_c = \left(\frac{\sigma}{E}\right)_s - \left(\frac{\sigma}{E}\right)_c$$

where $\delta\varepsilon$ = differential strain

ε = component strain

σ = component stress

E = component modulus of elasticity

subscripts designate superconductor (S) and copper (C)

positive strain corresponds to tensile stress

negative strain corresponds to compressive stress

We obtain a second equation from equilibrium. The longitudinal force in the copper must be equal and opposite to the longitudinal force in the N_bT_i

$$F_s + F_c = A_s\sigma_s + A_c\sigma_c = 0$$

solving for σ_s

$$(2)\quad \sigma_s = \frac{-A_c}{A_s}\,\sigma_c$$

where A_c/A_s is the copper superconductor ratio

Substituting equation (2) into equation (1) and solving for σ_c

$$(3)\quad \sigma_c = \frac{\delta\varepsilon}{\frac{A_c}{A_sE_s} + \frac{1}{E_c}}$$

Thermal strains due to a difference in length change of the components with respect to temperature change are treated in a similar manner.

$$(4) \quad \delta\varepsilon_T = \varepsilon_s - \varepsilon_c = \left[\frac{L_{RT} - L_T}{L_{RT}}\right]_s - \left[\frac{L_{RT} - L_T}{L_{RT}}\right]_c$$

where $\delta\varepsilon_T$ = differential thermal strain

L_T = component length at temperature

L_{RT} = component length at room temperature

Using equations (1) through (4) and a stress-strain curve for annealed copper the residual stresses in the wire components has been calculated for room temperature and liquid helium temperature. The results of these calculations for copper to superconductor ratios from 1 to 20 are shown in figure 1. These data show that the residual stresses remaining

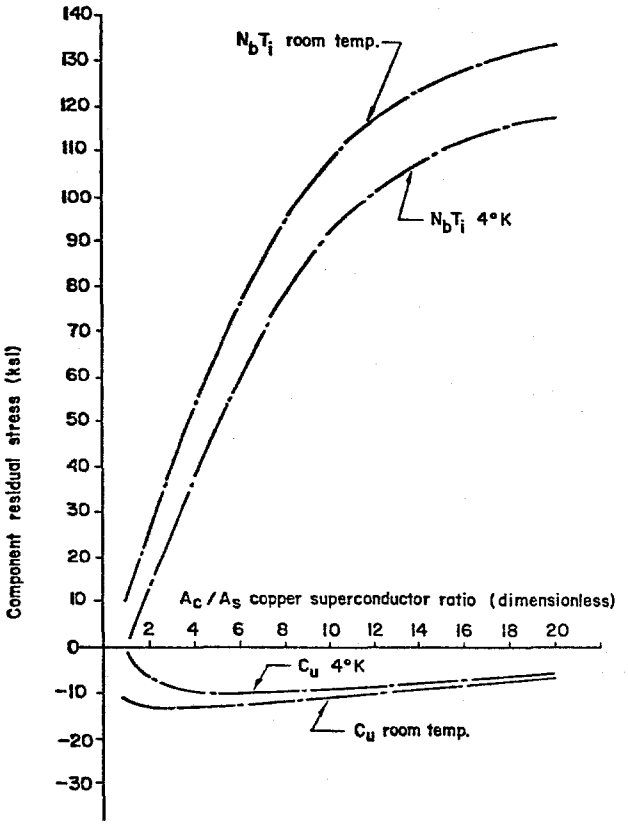

Fig. 1 Manufacturing Process Residual Stresses

in the wire components after the manufacturing process cannot be ignored and indicates that the stress-strain interactions between the components must be studied in detail. The reader should note that figure 1 is presented as qualitative data only in that assumptions have been made as to the process used by the manufacturer. A method of measuring the residual stresses in the components will be presented later and the measured data should be used as design criteria.

3 - Twisting

To evaluate the effects of twisting an expression was developed which describes the $N_b T_i$ stress distribution across the wire cross section with respect to axial strain.

$$(5) \quad \sigma_k = E_s \left[\frac{(\varepsilon + 1)^3}{(\varepsilon + 1)(n^2\pi^2 d_k^2 + 1)}\right]^{\frac{1}{2}} - E_s\left[\frac{(\varepsilon + 1)^3}{n^2\pi^2 d_k^2 + (\varepsilon + 1)^3}\right]^{\frac{1}{2}}$$

where n = number of twists per inch

ε = wire strain (axial)

d_k = circular element mean diameter

σ_k = circular element average stress

Equation (5) was then solved using numerical methods and the specimen wire data previously shown. The results

of these calculations are presented in figure 2. The error introduced by neglecting twisting effects in earlier calculations could be corrected by applying a 6% correction factor. Since previous calculations were intended to be qualitative only the correction is not considered significant. However, for later analysis using wire test data this correction will be applied by using an effective modulus of elasticity for $N_b T_i$ of .94 E_s.

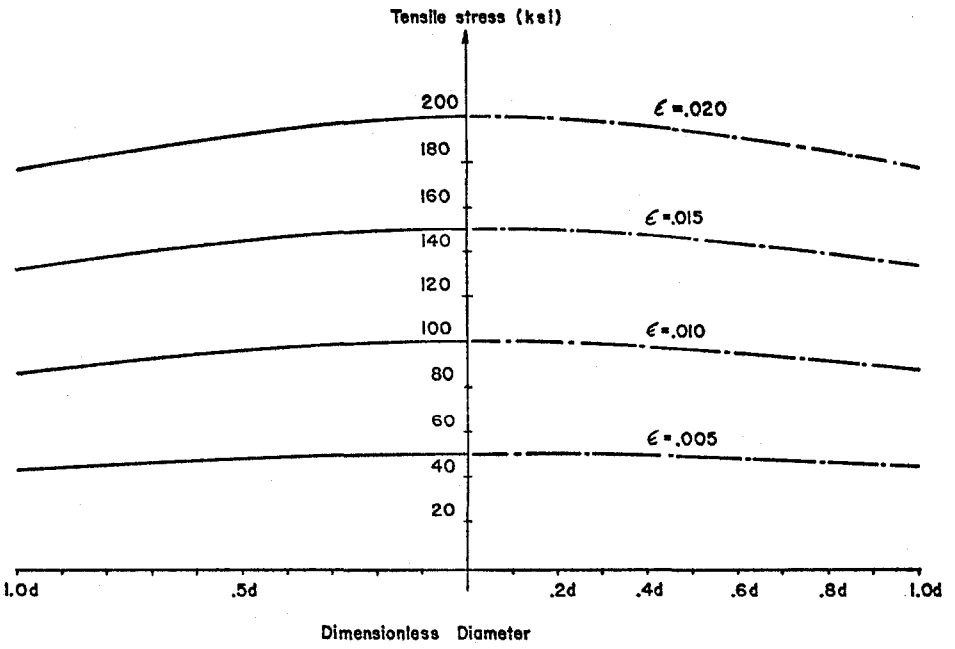

Fig. 2 $N_b T_i$ Diametral Stress Distribution

4 - Bending

Another manufacturing process which has a very important effect on superconducting coil performance is the inelastic strain introduced into the copper matrix by spooling and handling. If the wire is bent to some

radius of curvature smaller than R_{min} the copper component will exhibit inealstic behavior at the onset of tensile loading. This effect alone will be used later to explain a superconducting coil performance characteristic described as "training". The extreme fiber strain for a circular wire wrapped onto a spool may be expressed as

$$(6) \quad \varepsilon = \frac{\delta \ell}{\ell} = \frac{\pi(D + d) - \pi D}{\pi(D + d)} = \frac{d}{D + d}$$

where ε = extreme fiber strain

d = wire diameter

D = spool diameter

$\delta \ell$ = extreme fiber length change

ℓ = extreme fiber unstrained length

If we assume a maximum compressive prestress in the copper of 14,000 p.s.i. (see figure 1) due to previous manufacturing processes and a copper elastic limit in tension of zero (to be shown later) we can equate prestress strain to extreme fiber strain to determine R_{min}.

Note: The following expression is simplified by assuming that the neutral axis remains coincident with the area centroid.

$$(7) \quad \frac{d}{D + d} = \frac{[\sigma_c] \text{ prestress}}{E_c} = \frac{14{,}000}{18 \times 10^6}$$

the value of E_c is taken from reference 1

Solving for D

(8) $D = 1286d$

Equation 8 is interpreted in the following manner. If at any time during the final wire processing stages, handling, winding, etc. the wire is formed to a radius of curvature less than 643 wire diameters, the copper component will exhibit inelastic behavior only when tensile loading is applied.

Since our test specimen was delivered on a spool with a diameter much smaller than 1286d we will expect an inelastic stress-strain diagram during test.

The Bauschinger Effect

Another stress-strain interaction between wire components which may have an important effect on superconducting coil performance is the Bauschinger Effect.[2] If a material is loaded in tension beyond the elastic limit the elastic limit in tension is increased but the elastic limit in compression will be decreased. Similarly for compressive loading beyond the elastic limit the elastic limit in tension will be decreased. This effect will be used later to explain why poorly designed superconducting coils train to an upper limit which is lower than the design goals.

TESTS AND RESULTS

The stress-strain interactions between the superconducting wire components was studied in more detail with a straight forward tensile test. A wire specimen approximately 100 inches long was set up as shown in figure 3. Wire elongation was measured with a dial gage and the applied tensile load was measured with a spring balance. Typical load-deflection data for our specimen is presented in figure 4.

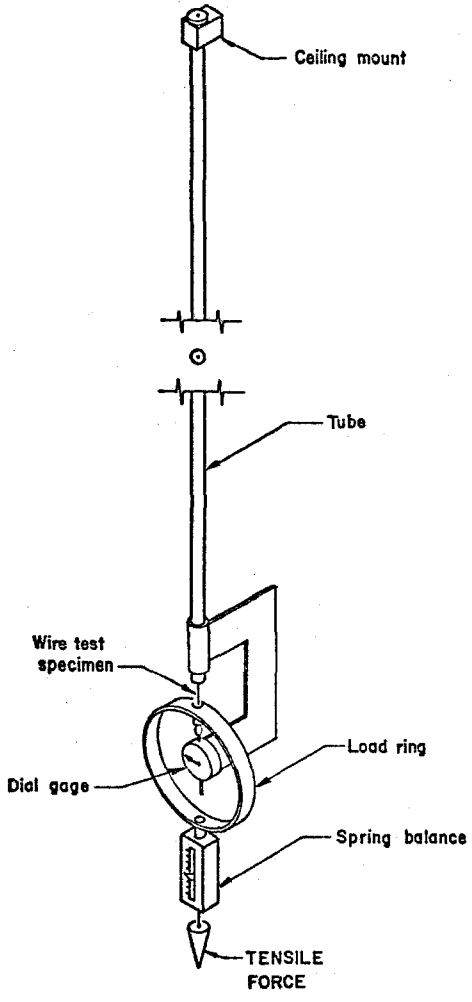

Fig. 3 Tensile Test Set Up

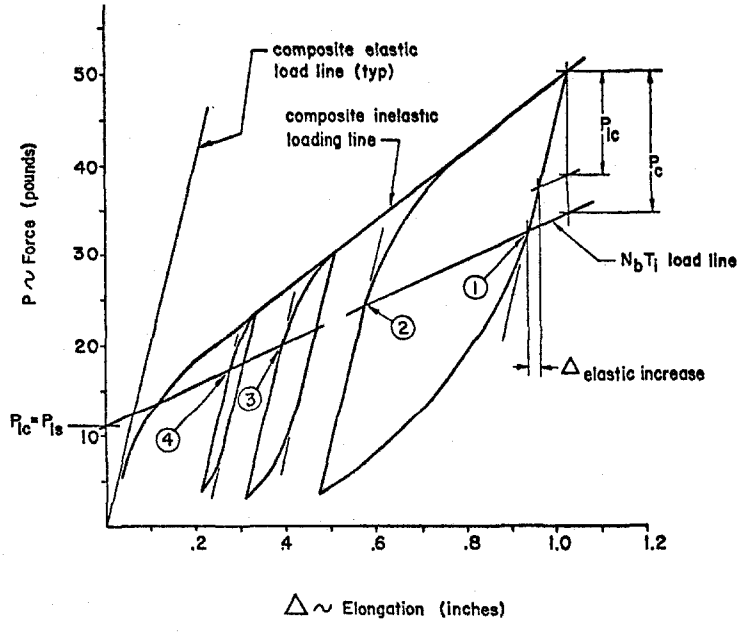

Fig. 4 Tensile Test Results

This data was obtained by loading the wire specimen in tension and unloading and reloading the wire to form the hysteresis loops shown. The modulus of elasticity and slope of the linear part of the composite wire load line is calculated as follows:

$$(9) \quad E_{comp} = \frac{A_c}{A_c + A_s}\left(E_c + .94\,\frac{A_s}{A_c}\,E_s\right)$$

$$\text{Slope} = \frac{P}{\Delta} = \frac{(A_c + A_s)E_{comp}}{\ell}$$

substituting (9) into above

$$(10) \quad \text{Slope} = \frac{A_cE_c + .94\,A_sE_s}{\ell}$$

where A = component cross-sectional area

.94 = twist correction factor discussed previously

ℓ = specimen original length

The slope of the loading and unloading lines were in good agreement with the slope calculated by equation (10) and they have been extended in figure 4 to show where the non-linear part of the hysteresis loop begins. A load line was also passed through the orgin to show that the wire behaves inelastically at the onset of tensile loading.

The next step in evaluating the test data was to determine what part of the applied load was carried by the N_bT_i. Since the N_bT_i behaves elastically the load line will be linear with a slope of

(11) $\text{slope} = \frac{P}{\Delta} = .94 \frac{A_s E_s}{\ell}$

The location of the $N_b T_i$ load line on the wire load-deflection plot was then determined by the following method. For the large hysteresis loop shown at the right in figure 4 point 1 is the transition from elastic to inelastic behavior of the composite wire for the unloading condition. Since the $N_b T_i$ behaves elastically point 1 must be the elastic limit of the copper in compression and the force transmitted through the $N_b T_i$ component must be greater than or equal to the applied load, i.e., the $N_b T_i$ load line must pass through point 1 or above it. Similarly, point 2 corresponds to the elastic limit of the copper in tension and the $N_b T_i$ load line must pass through point 2 or below it. The $N_b T_i$ load line was then added to figure 4 and the load line passed through both points 1 and 2. The $N_b T_i$ load line also passed through points 3 and 4 which are the elastic limits of the copper in tension for the smaller hysteresis loops. It then follows that the intersection of the $N_b T_i$ load line and the vertical coordinate is the tensile loading in the $N_b T_i$ for zero applied load and this value must be equal to the compressive load in the copper prior to specimen testing. For our specimen as shown in figure 4 the pre-loading in the copper component of the wire is 11 pounds which corresponds to a compression prestress in the copper of approximately 11,000 p.s.i. The agreement between this

measured value (11,000 p.s.i.) and the calculated value (see figure 1) is considered good for the assumptions made with respect to the manufacturing process.

The three hysteresis loops in figure 4 show the Bauschinger Effect very well. Precompression of the copper due to the manufacturing process has decreased the copper tension elastic limit of our specimen to zero and the copper component of our superconducting wire has an initial elastic strain capability of

$$(12) \quad \varepsilon_{elastic} = \frac{\sigma_{ic}}{E_c} = \frac{P_{ic}}{A_c E_c}$$

where subscript ic refers to initial copper and P_{ic} is the vertical intercept in figure 4.

Tensile loading and unloading of the specimen strain hardens the copper very little and the load reversal experienced by the copper shifts the tension and compression elastic limits of the copper such that Bauschinger loops are developed. The two smaller hysteresis loops show the copper compressive elastic limit to be decreasing (shifting toward the $N_b T_i$ load line) while the larger loop shows the cooper elastic limit to be reduced to its limiting value of zero.

Strain hardening effects are also apparent in figure 4. For the large hysteresis loop shown in figure 4 we see that the linear part of the wire unloading line is somewhat

longer than the linear part of the smaller loops. This increase in elastic strain capability is due to strain hardening of the copper. The increase in elastic strain capability may be calculated to be

$$(13) \quad \Delta\varepsilon_{\text{elastic}} = \frac{P_c + P_{ic}}{A_c E_c} \quad \text{for } |P_c| > |P_{ic}|$$

Note: for $|P_c| < |P_{ic}|$ the elastic strain capability is limited by the Bauschinger Effect to the value obtained using equation (12).

The increase in elastic elongation ($\Delta_{\text{elastic increase}}$) shown in figure 4 was then calculated to be

$$\Delta_{\text{elastic increase}} = \Delta\varepsilon_{\text{elastic}}\,\ell = \left(\frac{P_c + P_{ic}}{A_c E_c}\right)\ell = .018$$

Figure 4 shows the elastic elongation increase measured to be in good agreement with the strain hardening predicted by equation (13).

The next test was performed to study the effects of repeated cycles to see if the area and shape of the hysteresis loop degenerated. A new piece of the same superconducting wire was set up and the small loop shown in figure 4 was repeated 15 times with no significant change in the character of the loop. The only observed change was a gradual shifting of the loop to the right. This drifting to the right is probably due to copper creep. The next test was then performed to evaluate the same size loop at higher load levels

but the same strain excursion. This test would represent a coil designed to have the same strain excursion during operation with higher wire tension used to wind the coil. The test results are presented in figure 5. The first hysteresis loop generated was the small one which corresponds to a strain excursion of less than .1%. The larger loop was then generated with a strain excursion equal to the 15 cycle excursion. The loop area was then measured and found to be approximately 28% smaller in area than the loops generated at lower load levels. This area change was to be expected since $|P_c|$ was greater than $|P_{ic}|$ and the increase in the copper elastic strain capability decreases the loop area.

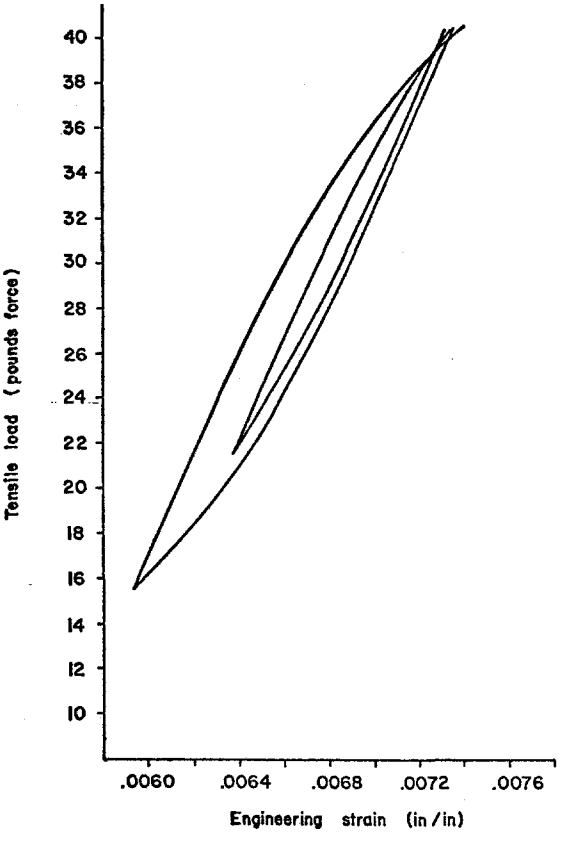

Fig. 5 Bauschinger Loops at Higher Load Levels

EVALUATION OF TEST RESULTS

To evaluate the heating potential of the above mechanical losses the thermal response of the superconducting wire is presented as a temperature rise independent of all other heating and cooling effects. Thermal calculations were simplified by assuming that the specific heat of N_bT_i is the same as copper for our temperature range and temperature-enthalpy data for copper was obtained from reference 3. The heating potential of the hysteresis loops shown in figures 4 and 5 was then calculated and the potential temperature rise (initial temperature of 4°K assumed) is shown in table 1.

TABLE 1

COIL THERMAL RESPONSE

Figure 4	heating potential (BTU/LB)	Potential Coil Temp. (°K)
Small loop	.00077	9.4°K
Intermediate loop	.0032	14°K
Large loop	.0231	23°K
Figure 5		
Small loop	.00031	7.3°K
Large loop	.00118	16.2°K

Further discussion as to the effect of mechanical losses on a specific coil design will not be discussed here since detailed coil analysis is beyond the scope of this paper. However, sample calculations for a superconducting solenoid coil constructed with our wire specimen showed mechanical losses to

be several times greater than electrical losses.

The next interpretation of our test results is a description of coil training which is due to inelastic behavior of the copper. The following description is considered qualitative only, i.e., a quantitative analysis must account for all heating and cooling peculiar to a specific coil design and operating system. Point 1 in figure 6 represents the initial condition of our wire specimen prior to charging the coil for the first time. When the coil is energized for the first time the copper experiences plastic deformation at the onset of tensile loading and proceeds to point 2 where the coil quenches. The wire then unloads along line 2-3 (slope given by equation 10) to point 3. When the coil is energized a second time the wire reloads along line 3-2 and then proceeds to point 4 where the coil quenches again. In this manner the coil continues to train to higher levels but the training gain becomes progressively smaller. The strain excursion eventually exceeds the initial elastic strain capability of the copper (equation 12)

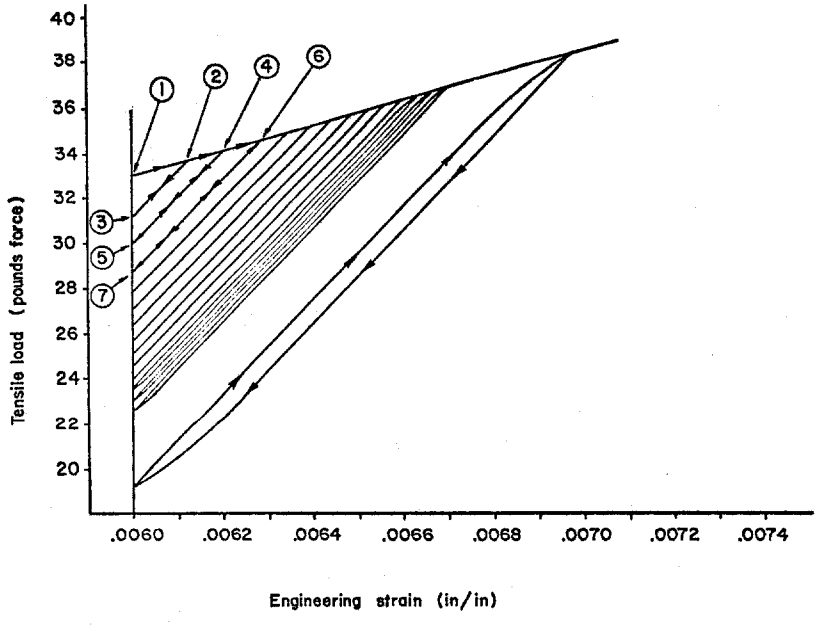

Fig. 6 Graphical Description of Training

and Bauschinger loops begin to develop. Finally, after many quenches the coil trains to its design value. The hysteresis loop shown in figure 6 represents the final Bauschinger loop for a coil designed to operate with a maximum strain excursion (hoop strain) of approximately .001 (see reference 4). For this example the coil has trained satisfactorily to full field, however, the coil performance may not be satisfactory if the charge time period is limited. Approximately half of the heat generated by the hysteresis loop is generated during the final 15% of the strain excursion at the end of the charge transient and this rate of heat generation may limit the charge time to longer periods than the design value. Finally, for poorly designed coils (see reference 4) severe Bauschinger loops may develop at currents and fields well below the design goals such that the coil will never reach its design values.

COIL DESIGN CONSIDERATIONS

1 - If forces are applied to a real material the material will experience deformations. Even if the boundaries of the coil (reaction members) approach infinite rigidity, the current conductors will still experience deformations when the coil is energized due to a redistribution of forces within the coil structure. One should not be misled into believing that prestressing will eliminate conductor motion. Prestressing may be used to limit conductor motion only.

2 - If prestressing is used to limit conductor motion, loss of preload due to relaxation of the coil and structure during construction and differential contractions due to cool down

should be evaluated.

3 - The elastic limits of the matrix metal used to stabilize the superconductor may be much lower than the yield strength. Stress analyses using standard engineering practice can result in a coil which is sound structurally but unsatisfactory thermally. Stress analysis only does not contribute to an understanding of coil stability. A detailed deflection analysis must be done and the heat generated by inelastic deformations must be accounted for if thermal stability is to be guaranteed.

4 - The stress-strain interactions between the metallic partners which make up the conductor composite must be studied in detail. A thorough understanding of these interactions identifies mechanical losses which have been neglected and establishes new "gound rules" for the development of coil designs which are mechanically stable.

5 - Coil parameter studies must be conducted which show the "trade-off" of all magnet thermal, structural, electrical and fluid flow parameters if optimum design is to be achieved. For example, sample calculations using the mechanical loss data presented herein show that the electrical losses in the copper are much lower than the mechanical losses for most coil designs. Therefore some cold working of the copper to increase its elastic strain capability should greatly improve coil performance and decrease the size of the reaction members, i.e., soft copper is not the best choice for an optimum design.

6 - The mechanical losses described herein may be eliminated by careful design and construction. The Bauschinger Effects

may be eliminated completely by strain hardening the copper a modest amount to increase its elastic strain capability. The coil designer can then measure the elastic strain capability of the finished wire to verify that the maximum strain experienced by the wire during coil operation is less than the measured value. The coil builder can also eliminate the inelastic copper losses associated with training by improving the stress distribution in the copper. The following discussion describes a method of accomplishing same after the coil is wound.

THE PWP PROCESS

The PWP process (post wind preload) has been invented[5] to change the stress distribution in the copper component of superconducting wire so that the copper will behave elastically during coil operation. After the coil has been completely wound a system of forces is applied to the coil and the strain experienced by the copper changes the stress distribution in the copper. In simple terms we might describe the process effect as a history eraser. The undesirable effects of spooling, handling, etc. are eliminated by prestressing the copper to a level greater than the operational stress. Figure 7 shows one method of performing the PWP process. The coil (solenoid shown) is wound on a mandrel made from a material which has a very low coefficient of expansion (invar or equivalent). After the coil is completely wound and cured (potted construction assumed) the coil with mandrel is cooled to 77°K with liquid nitrogen. Due to the contraction differential between copper and mandrel the copper component of the coil turns adjacent to the

bore will experience hoop strains approaching .3%. The coil is then warmed to room temperature and the mandrel is removed which completes the process.

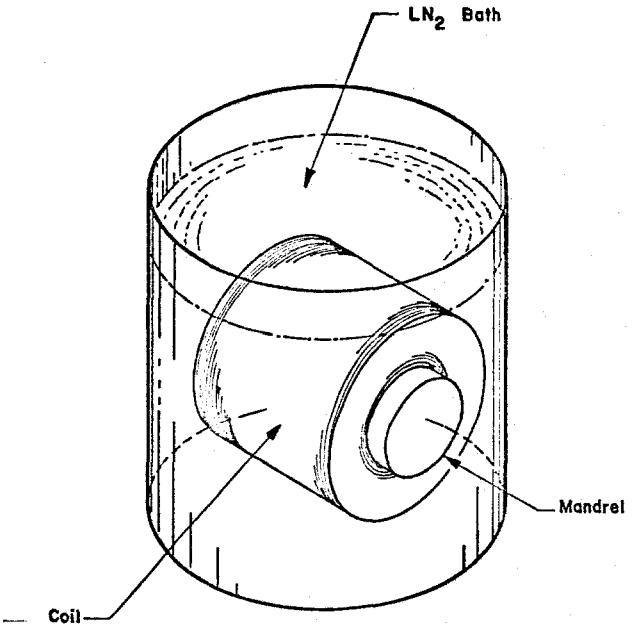

Fig. 7 The PWP Process

CONCLUSIONS AND FUTURE WORK

Inelastic behavior of the matrix metal used to stabilize superconductors should be treated as a mechanical loss which generates heat. These mechanical losses can be identified by material testing and eliminated with good design, careful construction and post wind preloading.

Electrical losses which generate heat during the charge and discharge transients may not be as great as previously measured[6] if mechanical losses were also present when electrical loss measurements were made. Future test coils designed to operate without mechanical losses should confirm this statement.

As soon as possible a superconducting solenoid test coil will be designed and built to verify that the above mechanical losses may be eliminated. The superconducting wire used to wind the test coil will be tensile tested at both room temperature and low temperatures. The coil performance test data will then be correlated with wire test results and detailed structure calculations to develop better coil design criteria.

Acknowledgements

The author wishes to acknowledge J. Jagger for his assistance in preparing the figures and H. Hart who helped with wire testing.

REFERENCES

1 Schwartzberg, F. R., et al, Cryogenic Materials Data Handbook, AD609562 (Martin Company, Denver, Colorado) latest revision August 1968, page F.1.ij

2 Timoshenko, S., Strength of Materials, Part II, Advanced Theory & Problems, Third Edition, pages 412-417

3 Properties of Materials at Low Temperatures, Phase I, Cryogenic Engineering Laboratory, Boulder, Colorado, page 4.112-1

4 Westendorp, W. F. & Kilb, R. W., Stresses in Magnetic Field Coils, Proceedings of the 1968 Summer Study on Superconducting Devices and Accelerators, Part III, page 723, figure 3, Radial Motion, page 726, figure 8

5 Record of Invention filed May 14, 1974, AEC Case number S-44, 379

6 W. B. Sampson, et al, Superconducting Synchrotron Magnets, Particle Accelerators, 1970, Vol. 1, page 173-185